

Article

Nonlinear Differential Braking Control for Collision Avoidance During Lane Change

Young Seop Son ¹ and Wonhee Kim ^{2,*} 

¹ Department of Robot and Smart Systems Engineering, Kyungpook National University, Daegu 702-70, Korea; ys.son@knu.ac.kr

² School of Energy Systems Engineering, Chung-Ang University, Seoul 156-756, Korea

* Correspondence: whkim79@cau.ac.kr; Tel.: +82-02-820-5928

Abstract: In this paper, a nonlinear differential braking control method is developed to avoid collision during lane change under driver torque. The lateral dynamics consist of lateral offset error and yaw error dynamics and can be interpreted as a semi-strict feedback form. In the differential braking control problem under the driver torque, a matching condition does not satisfy, and the system is not in the form of, the strict feedback form. Thus, a general backstepping control method cannot be applied. To overcome this problem, the proposed method is designed via the combination of the sliding mode control and backstepping. Two sliding surfaces are designed for differential braking control. One of the surfaces is designed considering the lateral offset error, and the other sliding surface is designed using the combination of the yaw and yaw rate errors as the virtual input of the lateral offset error dynamics. A brake steer force input is developed to regulate the two sliding surfaces using a backstepping procedure under the driver torque. Integral action and a super twisting algorithm are used in the lateral controller to ensure the robustness of the system. The proposed method, which is designed via the combination of the sliding mode control and backstepping, can improve the lateral control performance using differential braking. The proposed method is validated through simulations.

Keywords: differential braking; backstepping control



check for updates

Citation: Son, Y.S.; Kim, W. Nonlinear Differential Braking Control for Collision Avoidance During Lane Change. *Mathematics* **2021**, *9*, 1699. <https://doi.org/10.3390/math9141699>

Academic Editor: Nicu Bizon

Received: 10 June 2021

Accepted: 14 July 2021

Published: 19 July 2021

Publisher's Note: MDPI stays neutral with regard to jurisdictional claims in published maps and institutional affiliations.



Copyright: © 2021 by the authors. Licensee MDPI, Basel, Switzerland. This article is an open access article distributed under the terms and conditions of the Creative Commons Attribution (CC BY) license (<https://creativecommons.org/licenses/by/4.0/>).

1. Introduction

More than 90% of accidents on highways are caused by human error [1,2]. Particularly, in the case of fatal vehicular accidents, the collision between vehicles occurs during lane change [3]. Various systems that provide a prior warning to the driver attempting to change a lane under the risk of collision have been developed to avoid such accidents. Additionally, several methods for risk assessment have been investigated [4–8]. Jula et al. [4] studied the kinematics of vehicles involved in a lane changing/merging maneuver and provided conditions under which lane changing/merging crashes can be avoided. Collision risks are estimated as stochastic variables and are predicted for a short period ahead by using hidden Markov models and Gaussian processes [5]. A method that propagates the known error covariance matrix of the current pose of the ego vehicle by considering local approximations of the predicted trajectory was proposed in [6]. In [7], a collision risk assessment algorithm was developed via lane-based probabilistic motion prediction of surrounding vehicles. A situational assessment based on Stochastic model and Gaussian distributions was designed for intelligent vehicles [8]. These systems cannot actively help a driver to avoid a collision. Therefore, systems that utilize steering torque and provide active assistance to avoid collisions have been developed [9–11] for power steering systems. Integrated steering and differential braking methods were developed for emergency collision avoidance [12–14]. However, the steering interaction between the driver and the controller was not considered in these methods. The torque imposed by the controller in the power steering systems can

lead to discomfort while driving and result in negative effects such as overlapped steering torque imposed by the driver and the controller [15].

Alternatively, lateral position control methods were proposed. These use differential brake forces for steering intervention [15–19]. In [16], the usefulness of a brake steer system that uses differential brake forces for steering intervention was studied. A surface sliding controller with a weighted combination of yaw rate, nominal yaw rate error, and lateral offset error (or sideslip angle) was proposed [17,18]. A blind spot intervention (BSI) system was developed by Infinity [19]. The BSI system uses selective brake application to steer the car back to the center of the lane and avoids collision if a vehicle is present in the blind spot or vice versa. A hierarchical lane-keeping assistance control algorithm for a vehicle was proposed in [15]. The lateral dynamics where the brake steer force is the system input are not in the form of the strict feedback system. Therefore, the backstepping control scheme cannot be applied to lateral dynamics with the brake steer force input [20–22]. Hence, the weighted combination of the lateral offset error (or sideslip angle) and the yaw rate error is widely used as the sliding surface for the sliding mode control [17,18]. However, the simultaneous regulation of the yaw rate error and lateral offset error cannot be guaranteed by using the sliding surface used in the previous studies. Furthermore, in the differential braking control problem under the driver torque, matching condition does not satisfy and the system is not in the form of the strict feedback system. Thus, general backstepping control method cannot be applied. Therefore, it is crucial to design a control method for the regulation of both the yaw rate error and the lateral offset error.

In this study, a nonlinear differential braking control method is developed to avoid collision during lane change under driver torque. The lateral dynamics consist of lateral offset error and yaw error dynamics and can be interpreted as a semi-strict feedback form. Two sliding surfaces are designed for differential braking control. One of the sliding surface surfaces is designed in terms of the lateral offset error, and the other sliding surface is designed using the combination of the yaw and yaw rate errors as the virtual input of the lateral offset error dynamics. The brake steer force input is developed to regulate two sliding surfaces using the backstepping procedure under the driver torque. The proposed method designed via the combination of the sliding mode control and the backstepping can improve the lateral control performance using differential braking. Integral action and super twisting algorithm are used in the lateral controller to ensure robustness of the system. The performance of the proposed method is validated through simulations.

2. Vehicle Lateral Dynamics Modeling

The detailed dynamics of a vehicle including longitudinal and lateral dynamics can be described using mechanical model that naturally has a minimum of six degrees of freedom (DOF) [23–25]. The bicycle model as shown in Figure 1 is used for lateral vehicle dynamics. The lateral position error, lateral position error at the lookahead distance point, heading angle, and reference trajectory are described in Figure 2. In Figures 1 and 2, $\{XYZ\}$ is a inertial coordinate frame, $\{xyz\}$ is a local coordinate frame, x is a longitudinal position of the origin of the $\{xyz\}$ coordinate to the front fixed point, y is a lateral position of the origin of the $\{xyz\}$ coordinate to the rotation center 'O' along the lateral axis, V is a velocity at c.g. of vehicle, $\dot{x} = V_x$ is a longitudinal velocity at c.g. of vehicle, $\dot{y} = V_y$ is a lateral velocity at c.g. of vehicle, I_z is a yaw moment of inertia of vehicle, l_f and l_r are longitudinal distances from c.g. to front and rear tires, respectively, ψ is a yaw, heading, angle of vehicle in global axis, β is a vehicle slip angle at c.g. of vehicle, α_f and α_r are slip angles at front and rear wheel tires, respectively, δ is a steering angle, F_{yf} and F_{yr} are lateral tire forces on front and rear tires, respectively, R is a turning radius of vehicle or radius of road, L is a look-ahead distance from c.g. to look-ahead point, e_y is a lateral offset error with respect to reference, and e_ψ is a yaw angle error with respect to road.

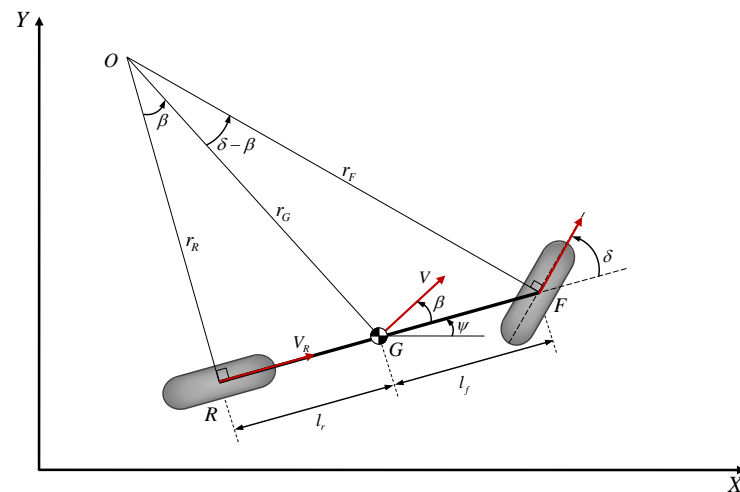


Figure 1. Bicycle model diagram of lateral vehicle dynamics.

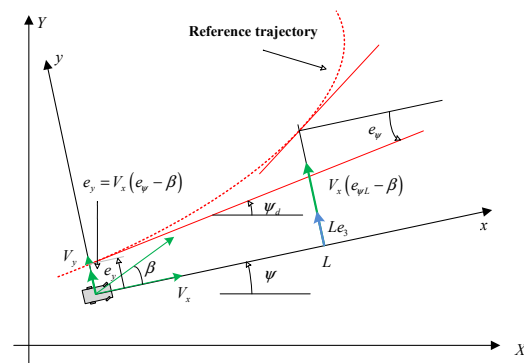


Figure 2. Lateral position and velocity errors at the look-ahead distance point.

We define the error states e for the lateral control as

$$e = \begin{bmatrix} e_1 \\ e_2 \\ e_3 \\ e_4 \end{bmatrix} = \begin{bmatrix} y - y_d \\ \dot{y} - \dot{y}_d \\ \psi - \psi_d \\ \dot{\psi} - \dot{\psi}_d \end{bmatrix} \tag{1}$$

where e_1 is the lateral offset error, e_3 is the yaw error, y is the lateral offset, y_d is the desired lateral offset, ψ is the yaw, and ψ_d is the desired yaw. The basic lateral model is described in terms of the lateral offset at the vehicle's center of gravity and convert it in terms of the lateral offset at the look-ahead distance. The error dynamics in terms of the state vector are then obtained as

$$\dot{e} = \begin{bmatrix} 0 & 1 & 0 & 0 \\ 0 & a_{22} & a_{23} & a_{24} \\ 0 & 0 & 0 & 1 \\ 0 & a_{42} & a_{43} & a_{44} \end{bmatrix} e + \begin{bmatrix} 0 \\ 0 \\ 0 \\ b_{F4} \end{bmatrix} F_{bs} + \begin{bmatrix} 0 \\ b_{\delta 2} \\ 0 \\ b_{\delta 4} \end{bmatrix} \delta + \begin{bmatrix} 0 \\ b_{w2} \\ 0 \\ b_{w4} \end{bmatrix} \dot{\psi}_d \tag{2}$$

where F_{xfl} and F_{xfr} are longitudinal tire forces at front left and right tire, respectively, $F_{bs} = F_{xfl} - F_{xfr}$ is a brake steer force and a control input, m is a total mass of vehicle, w_i is a width of the vehicle, $C_{\alpha f}$ and $C_{\alpha r}$ are cornering stiffness of front and rear tires, respectively,

$$a_{22} = -\frac{2C_{\alpha f} + 2C_{\alpha r}}{mV_x}, \quad a_{23} = -a_{22}V_x,$$

$$a_{24} = -\frac{2C_{\alpha f}l_f - 2C_{\alpha r}l_r}{mV_x}, \quad a_{42} = -\frac{2C_{\alpha f}l_f - 2C_{\alpha r}l_r}{I_z V_x},$$

$$\begin{aligned}
 a_{43} &= -a_{42}V_x, & a_{44} &= -\frac{2C_{\alpha f}l_f^2 + 2C_{\alpha r}l_r^2}{I_z V_x}, \\
 b_{F4} &= \frac{w_t}{2I_z}, & b_{\delta 2} &= \frac{2C_{\alpha f}}{m}, & b_{\delta 4} &= \frac{2C_{\alpha f}l_f}{I_z}. \\
 b_{w2} &= -\frac{2C_{\alpha f}l_f - 2C_{\alpha r}l_r}{I_z V_x} - V_x, & b_{w4} &= -\frac{2C_{\alpha f}l_f^2 + 2C_{\alpha r}l_r^2}{I_z V_x}.
 \end{aligned}$$

The detailed mathematical modeling for (2) is discussed in [24,25]. We rewrite the error dynamics (2) as

$$\begin{aligned}
 \dot{e}_1 &= e_2 \\
 \dot{e}_2 &= a_{22}e_2 + a_{23}e_3 + a_{24}e_4 + b_{\delta 2}\delta + b_{w2}\dot{\psi}_d \\
 \dot{e}_3 &= e_4 \\
 \dot{e}_4 &= a_{42}e_2 + a_{43}e_3 + a_{44}e_4 + b_{\delta 4}\delta + b_{w4}\dot{\psi}_d + b_{F4}F_{bs}.
 \end{aligned} \tag{3}$$

If both δ and $\dot{\psi}_d$ are zero without the input F_{bs} , the equilibrium point is $e = [a, 0, 0, 0]^T$ where a is a constant. If δ and/or $\dot{\psi}_d$ are not zero, e_3 of the equilibrium point cannot be zero for the compensation of δ and/or $\dot{\psi}_d$ in \dot{e}_2 . On a straight road, the desired yaw rate $\dot{\psi}_d$ is zero. When the driver tries to change the lane, the steering wheel angle δ becomes nonzero so that e_3 cannot be zero although e_1 is kept to be zero by the control input F_{bs} . The aim of the controller design is to determine the brake steer force F_{bs} such that

$$\lim_{t \rightarrow \infty} e_1(t) = 0. \tag{4}$$

when the driver changes a lane under the collision risk. The steering angle δ that is activated as the disturbance in the differential braking system is in both e_2 and e_4 dynamics. Furthermore, the error dynamics (3) is not in the form of the strict feedback system. Thus, general nonlinear control methods such as the sliding mode control, the backstepping control cannot be used for the error dynamics (3). To overcome this problem, the proposed method is designed via the combination of the sliding mode control and the backstepping.

3. Control Strategy for Collision Avoidance

3.1. Structure of the Collision Avoidance System

The overall architecture of the side crash avoidance system is depicted in Figure 3. The algorithm consists of the following three parts. (1) The driver's lane change intention and the vehicle status are checked via sensor fusion [26,27], and the collision risk is determined and the presence of a vehicle in the blind spot is checked [6,28]. (2) If the driver's lane change intention is detected under the collision risk with a vehicle in the target lane or with a vehicle in the blind spot, the system warns the driver about the collision risk and the lateral control system is turned on. (3) The differential braking input calculated to ensure regulation of the lateral offset error, lateral offset error rate, yaw, and yaw rate by the differential braking control method maintains the vehicle on the original lane. In this paper, we focus on the design of the differential braking control method to maintain the vehicle on the original lane.

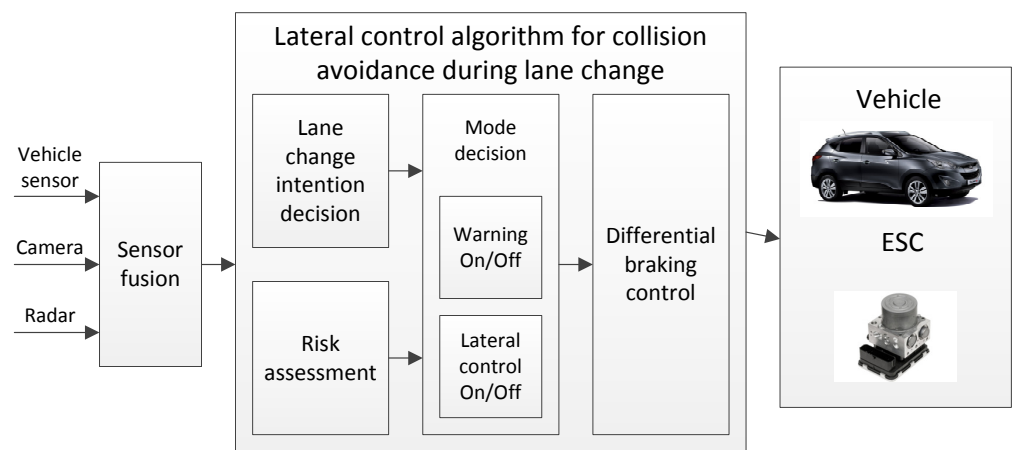


Figure 3. Architecture of the collision avoidance system.

3.2. Strategy of Lateral Control for Collision Avoidance

A strategy of the lateral control to avoid collision with a vehicle in the target lane is shown in Figure 4. The driver starts to change the lane at t_0 . At t_1 , the risk assessment predicts a collision, and the system warns the driver about the collision risk. Additionally, the brake steer force is generated by the control algorithm to prevent lane change. The driver tries to return to the original lane at t_2 . If the lateral offset error e_1 , yaw error e_3 , and steering wheel angle δ are considerably small, the differential braking control is released.

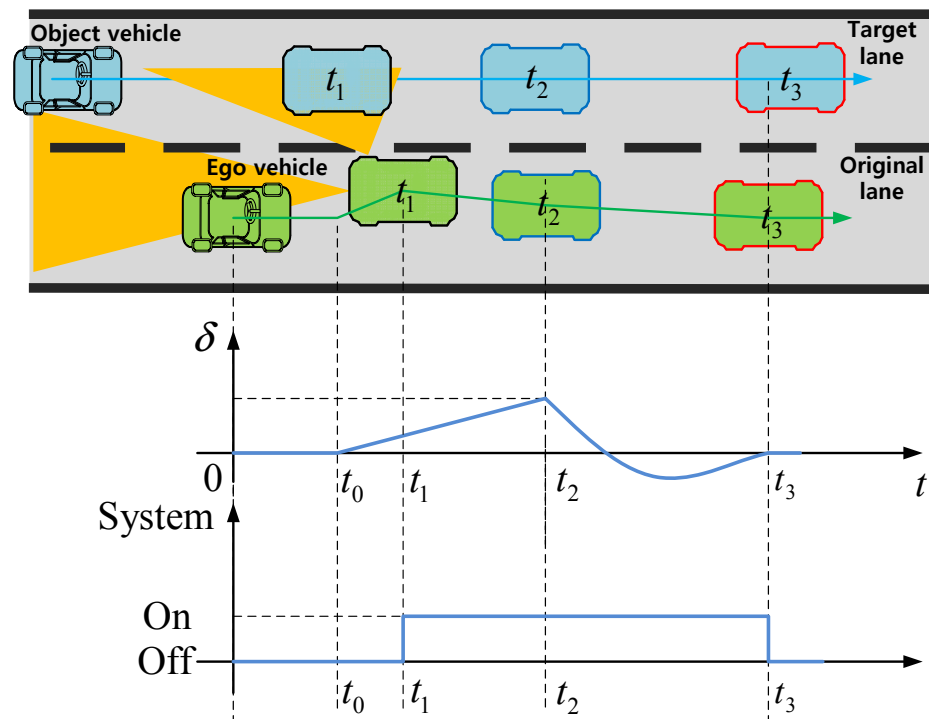


Figure 4. Strategy of the lateral control for the avoidance of the side crash.

4. Differential Braking Control Algorithm Design for Lateral Control

To eliminate steady-state error, integrator error e_0 is defined as

$$e_0 = \int_0^t e_1 d\tau. \tag{5}$$

Thus, the error dynamics (3) can be written as

$$\begin{aligned} \dot{e}_0 &= e_1 \\ \dot{e}_1 &= e_2 \\ \dot{e}_2 &= a_{22}e_2 + a_{23}e_3 + a_{24}e_4 + b_{\delta 2}\delta + b_{w2}\dot{\psi}_d \\ \dot{e}_3 &= e_3 \\ \dot{e}_4 &= a_{42}e_2 + a_{43}e_3 + a_{44}e_4 + b_{\delta 4}\delta + b_{w4}\dot{\psi}_d + b_{F4}F_{bs}. \end{aligned} \tag{6}$$

The error dynamics (6) consist of lateral offset error dynamics and yaw error dynamics and it can be interpreted as a semi-strict feedback form as follows:

$$\begin{aligned} \dot{e}_0 &= e_1 \\ \dot{e}_1 &= e_2 \\ \dot{e}_2 &= f_2(e_2) + g_2^T e_b + b_{\delta 2}\delta + b_{w2}\dot{\psi}_d \\ \dot{e}_b &= f_b(e) + g_u b_{F4}F_{bs} + g_d^T d \end{aligned} \tag{7}$$

where $e_b = [e_3, e_4]^T$, $d = [\delta, \dot{\psi}_d]^T$, $f_2(e_2) = a_{22}e_2$, $g_2 = [a_{23}, a_{24}]^T$, $g_u = b_{F4}$, $f_b(e) = \begin{bmatrix} e_3 \\ a_{42}e_2 + a_{43}e_3 \end{bmatrix}$, $g_d = [b_{\delta 4}, b_{w4}]^T$. In (6), the lateral offset error dynamics are

$$\begin{aligned} \dot{e}_0 &= e_1 \\ \dot{e}_1 &= e_2 \\ \dot{e}_2 &= a_{22}e_2 + a_{23}e_3 + a_{24}e_4 + b_{\delta 2}\delta + b_{w2}\dot{\psi}_d. \end{aligned} \tag{8}$$

Considering lateral offset error dynamics (8), the term $a_{23}e_3 + a_{24}e_4$ can be regarded as the virtual input. Two sliding surfaces s_1 and s_2 are designed for the controller design. The sliding surface s_1 is designed in terms of the lateral offset error as

$$s_1 = \sigma_0 e_0 + \sigma_1 e_1 + e_2 \tag{9}$$

where the coefficients σ_0 and σ_1 are chosen such that the polynomial $s^2 + \sigma_1 s + \sigma_0$ is Hurwitz. For the virtual input of the lateral offset error dynamics (8), the sliding surface s_2 is defined as

$$s_2 = a_{23}e_3 + a_{24}e_4. \tag{10}$$

Then, the lateral offset error dynamics (8) become

$$\begin{aligned} \dot{e}_0 &= e_1 \\ \dot{e}_1 &= e_2 \\ \dot{e}_2 &= a_{22}e_2 + s_2 + b_{\delta 2}\delta + b_{w2}\dot{\psi}_d. \end{aligned} \tag{11}$$

From (8) and (9), we obtain \dot{s}_1 as

$$\dot{s}_1 = \sigma_0 e_1 + \sigma_1 e_2 + a_{22}e_2 + s_2 + b_{\delta 2}\delta + b_{w2}\dot{\psi}_d. \tag{12}$$

For the convergence of the sliding surface s_1 to the zero, the reference of s_2 is designed as

$$s_{2d} = -\sigma_0 e_1 - \sigma_1 e_2 - a_{22}e_2 - b_{\delta 2}\delta - b_{w2}\dot{\psi}_d - k_1 s_1. \tag{13}$$

Equation (12) thus becomes

$$\dot{s}_1 = -k_1 s_1 + z_2 \tag{14}$$

where z_2 is the tracking error for s_2 as $z_2 = s_2 - s_{2d}$. The derivative of z_2 with respect to time is

$$\begin{aligned} \dot{z}_2 &= \dot{s}_2 - \dot{s}_{2d} \\ &= a_{23}e_4 + a_{24}\dot{e}_4 - \dot{s}_{2d} \\ &= a_{23}e_4 + a_{24}(a_{42}e_2 + a_{43}e_3 + a_{44}e_4 + b_{\delta 4}\delta + b_{w4}\dot{\psi}_d) + a_{24}b_{F4}F_{bs} - \dot{s}_{2d}. \end{aligned} \tag{15}$$

The input is designed as

$$\begin{aligned} u &= -\frac{1}{a_{24}b_{F4}}[a_{23}e_4 + a_{24}(a_{42}e_2 + a_{43}e_3 + a_{44}e_4)] \\ &\quad - \frac{1}{a_{24}b_{F4}}[a_{24}(b_{\delta 4}\delta + b_{w4}\dot{\psi}_d) - \dot{s}_{2d} + \phi_1(z_2) - \phi_2(z_2)] \end{aligned} \tag{16}$$

where $\phi_1(z_2) = k_{z1}|z_2|^{\frac{1}{2}}\text{sgn}(z_2)$, $\phi_2(z_2) = -k_{z2}\text{sgn}(z_2)$, k_2 and k_s are positive constant.

Theorem 1. Suppose the error dynamics (3) with the control law (13) and (16). The lateral offset error e_1 converges to zero and the yaw error e_3 is bounded. With $\delta = \dot{\psi}_d = 0$, the yaw error e_3 converges to zero.

Proof. Step 1: From (14),

$$\dot{s}_1 = -k_{s1}s_1 + z_2. \tag{17}$$

The energy function V_1 is defined as

$$V_1 = \frac{1}{2}s_1^2. \tag{18}$$

Then, \dot{V}_1 is obtained as

$$\dot{V}_1 = -k_{s1}s_1^2 + z_2s_1. \tag{19}$$

In (17), z_2 and s_1 are regarded as the input and the output, respectively. Then, (19) can be rewritten as

$$\underbrace{z_2}_{input} \underbrace{s_1}_{output} = \dot{V}_1 + \underbrace{k_{s1}s_1^2}_{\geq 0}. \tag{20}$$

From (20), the relationship between s_1 and z_2 is strictly output passive [29] and $\dot{s}_1 = -k_{s1}s_1$ is zero-state observable. Therefore, s_1 system is input-to-state stable. With control law (16), the dynamics of z_2 and ϕ_2 are

$$\begin{aligned} \dot{z}_2 &= -k_{z1}|z_2|^{\frac{1}{2}}\text{sgn}(z_2) + \phi_2 \\ \dot{\phi}_2 &= -k_{z2}\text{sgn}(z_2). \end{aligned} \tag{21}$$

With the definition of the vector $\zeta = [\zeta_1 \ \zeta_2]^T = [|z_2|^{\frac{1}{2}}\text{sgn}(z_2), \phi_2]^T$, ζ dynamics are

$$\dot{\zeta} = \frac{1}{|\zeta_1|}A_\zeta\zeta \tag{22}$$

where $A_\zeta = \begin{bmatrix} -\frac{1}{2}k_{z1} & \frac{1}{2} \\ -k_{z2} & 0 \end{bmatrix}$ and $|\zeta_1| = |z_2|^{\frac{1}{2}}$. With $k_{z1} > 0$ and $k_{z2} > 0$, A_ζ is Hurwitz. The Lyapunov candidate function V_ζ is defined as

$$V_\zeta = \zeta^T P_\zeta \zeta \tag{23}$$

where P_ζ is positive definite. The derivative of ζ with respect to time is given by

$$\dot{V}_\zeta = -\frac{1}{|\zeta_1|} \zeta^T Q_\zeta \zeta \tag{24}$$

where Q_ζ is positive definite such that $A_\zeta^T P_\zeta + P_\zeta A_\zeta = -Q_\zeta$. Thus, the origin $\zeta = 0$ is finite time stable. Consequently z_2 converges to zero in finite time.

Step 2: With $z_2 = 0$, s_1 in (17) is obtained as

$$\dot{s}_1 = -k_{s1}s_1. \tag{25}$$

Then, with the definition of s_1 (9), (11) can be rewritten as

$$\begin{aligned} \dot{e}_0 &= e_1 \\ \dot{e}_1 &= e_2 \\ e_2 &= -\sigma_0 e_0 - \sigma_1 e_1 + s_1. \end{aligned} \tag{26}$$

Equation (26) can then be rewritten as

$$\dot{e}_a = A_a e_a + B_a s_1 \tag{27}$$

where $e_a = [e_0, e_1]^T$, $A_a = \begin{bmatrix} 0 & 1 \\ -\sigma_0 & -\sigma_1 \end{bmatrix}$, $B_a = [0, 1]^T$. Because A_a is Hurwitz, e_a is bounded-input bounded output (BIBO) stable. With the convergence of s_1 to zero, e_0 and e_1 converge to zeros. Furthermore, $e_2 = -\sigma_0 e_0 - \sigma_1 e_1 + s_1$ also converges to zero.

Step 3: With $z_2 = 0$,

$$s_2 = s_{2d}. \tag{28}$$

From (3), (10), and (28), we obtain

$$\begin{aligned} \dot{e}_3 &= e_4 \\ a_{24}e_4 &= -a_{23}e_3 + \tilde{\zeta}. \end{aligned} \tag{29}$$

where $\tilde{\zeta} = -\sigma_0 e_1 - \sigma_1 e_2 - a_{22}e_2 - b_{\delta 2}\delta - b_{w2}\dot{\psi}_d - k_1 s_1$. As e_0, e_1 , and e_2 converge to zeros, $\tilde{\zeta}$ is bounded in the transient response. δ and $\dot{\psi}_d$ are also bounded. Thus a positive constant $\tilde{\zeta}_{\max}$ exists such that $\tilde{\zeta}_{\max} = \sup_t \tilde{\zeta}(t)$. Equation (29) is thus simplified as

$$\dot{e}_3 = -\frac{a_{23}}{a_{24}}e_3 + \frac{\tilde{\zeta}}{a_{24}}. \tag{30}$$

From (30), we have

$$|e_3(t)| \leq \exp\left(-\frac{a_{23}}{a_{24}}t\right) |e_3(0)| + \frac{1}{a_{24}} \tilde{\zeta}_{\max} \tag{31}$$

e_0, e_1, e_2 converge to zeros. For a straight load, $\dot{\psi}_d$ is zero. With $\delta = 0$, $\tilde{\zeta}$ converges to zero, then, e_3 converges to zero. Consequently, e_4 also converges to zero. \square

The block diagram of the proposed method is shown in Figure 5. The sliding surfaces (9) and (10) are calculated by using the error feedback. Then the control input (16) is obtained, then is applied to the lateral error dynamics (3).

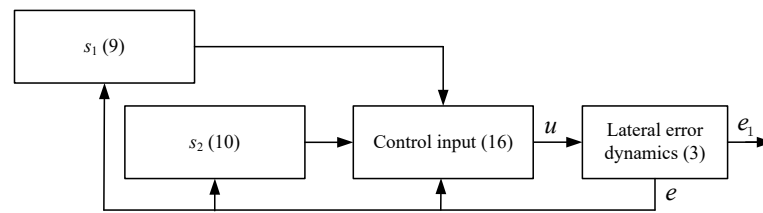


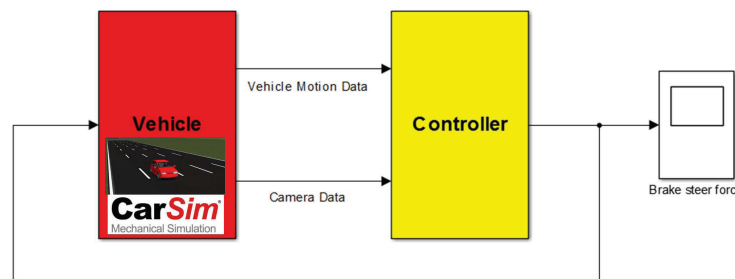
Figure 5. Block diagram of the proposed method.

5. Simulation Results

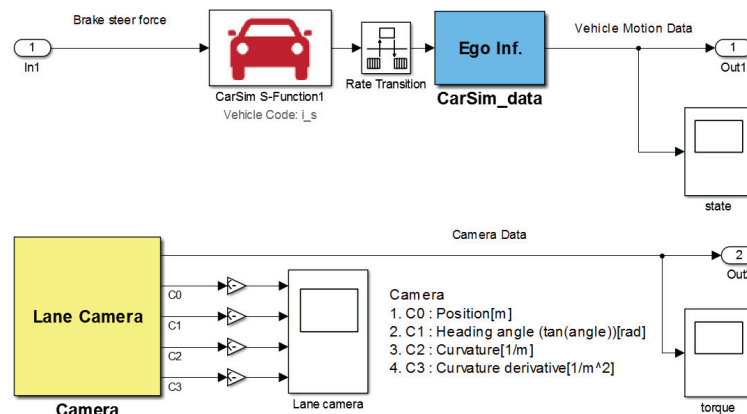
The proposed method was tested via a simulation. Simulations were performed using the vehicle dynamic software CarSim and Matlab/Simulink as shown in Figure 6. The S-function coded in C language was used for implementing the proposed control method. The vehicle dynamics were performed using CarSim, which allows high-order vehicle dynamics including yaw, roll, and pitch motions. The camera data were obtained using CarSim data and the lane polynomial $f_L(x)$ defined as a third order polynomial function of the longitudinal distance, x [30]

$$f_L(x) = c_0 + c_1 \cdot x + c_2 \cdot x^2 + c_3 \cdot x^3 \tag{32}$$

where c_0 is the lateral offset, c_1 is the head angle, c_2 is the curvature, and c_3 is the curvature rate. From c_0 and c_1 , the lateral offset and yaw errors are obtained. The parameters used in the simulation were the nominal values of a test vehicle. The control parameters for (9), (10), and (16) are listed in Table 1.



(a) Overall simulation structure that consists of CarSim vehicle model



(b) Vehicle part. The output of lane camera is lane coefficients; c_0 denotes the lateral lane center offset at c.g., c_1 denotes the in-lane heading slop, the heading angle error at c.g., c_2 denotes curvature/2 at $s = 0$ and c_3 denotes the curvature-rate/6

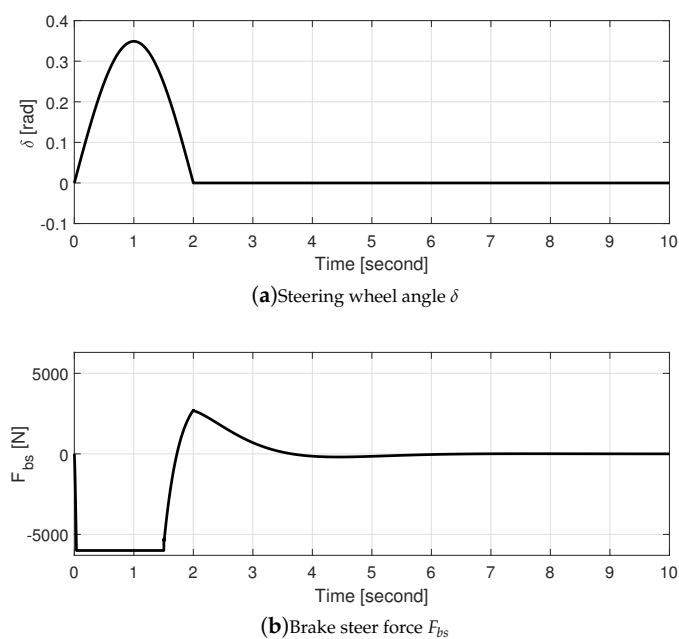
Figure 6. Vehicle and camera models used in the simulations.

Table 1. Control Parameters used in (9), (10), and (16).

Parameter	Value	Parameter	Value
σ_0	1,000,000	σ_1	200
σ_3	50	σ_4	0
k_1	1	k_2	1
K_s	0.1		

5.1. Straight Road

In these simulations, the straight road was used. For the straight road, the test scenario demonstrated in Figure 4 was used. The test scenario is as follows: (1) at 0 s, the driver attempts lane change; (2) at 1 s, there is a collision risk with the object vehicle in the target lane; (3) the differential braking control system is activated to avoid the collision risk at 1 s; and (4) the differential braking control system operates to move the vehicle to the center of the original lane. The speed of the vehicle was 80 km/h on a straight road. The simulation results are shown in Figures 7–10. The steering wheel angle increased which signifies that the driver attempted lane change. Thus, the errors increased for the lane change. At 1 s, the system warned the driver about the collision risk and the lateral control system was turned on. Since the driver detected collision risk at 1 s, the steering wheel angle decreased after 1 s. The differential braking control system was activated to avoid the collision risk at 1 s. The differential braking control input was applied to the system for regulating the lateral offset error with the steering angle compensation. Thus, after 1 s of it starting, the errors were reduced by the differential braking input, although δ was positive. At 6 s, since the steering angle and lateral offset error are considerably small, the differential braking control system was turned off. The sliding surface s_1 and the surface tracking error z_2 are shown in Figure 10. It was observed that both s_1 and z_2 converged to zero. Figure 11 shows the vehicle trajectory of the proposed method. The dash-line represented the lane of the ego vehicle. We see that the proposed method maintained the vehicle on the original lane under the steering angle for the lane change.

**Figure 7.** Steering angle and Brake steer force.

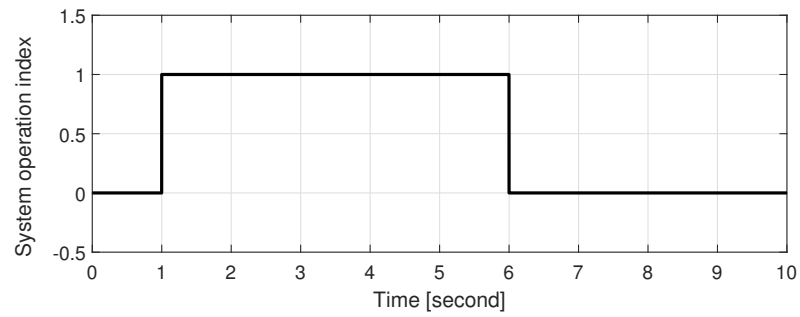
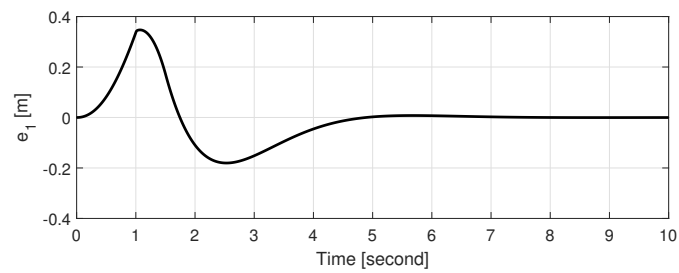
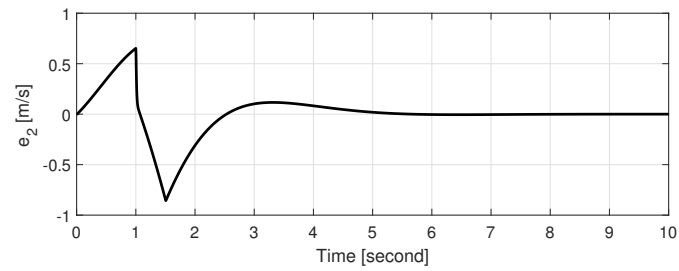


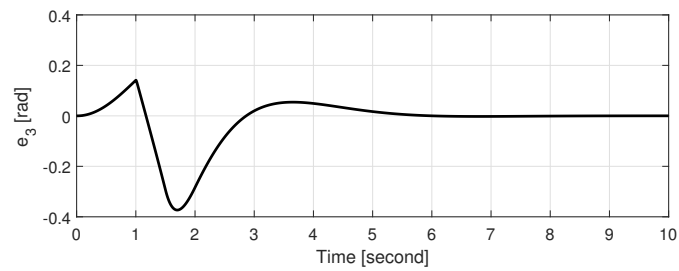
Figure 8. System operation index.



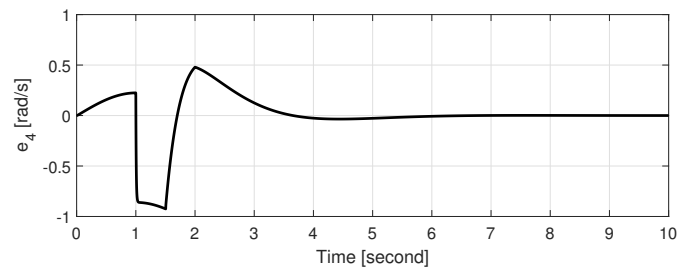
(a) Lateral offset error e_1



(b) Derivative of the lateral offset error e_2



(c) Yaw error e_3



(d) Yaw rate error e_4

Figure 9. Lateral offset and yaw errors.

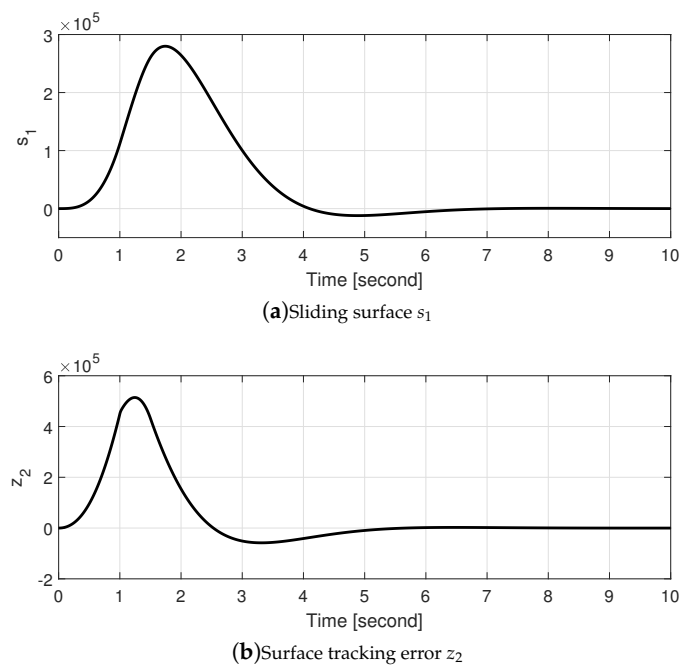


Figure 10. Sliding surface s_1 and surface tracking error z_2 .

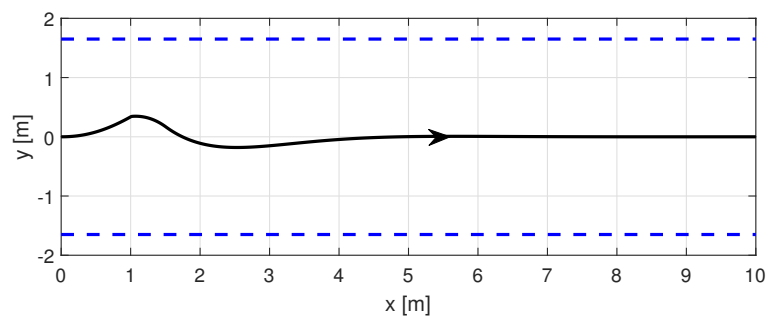


Figure 11. Vehicle trajectory of the proposed method.

5.2. Curved Road

To validate the performance of the proposed method, the comparison between the proposed method and the proportional-integral (PI) control method was tested for the curved road. The curved road as shown in Figure 12 was used for the simulation. Two vehicles drove on the curved road side by side. It was impossible that the ego vehicle changes the lane change. Despite collision risk, the driver tried the lane change on the curved road at 6 s and 11 s as shown in Figure 13, twice times, thus, the differential braking control system operated for the collision avoidance from 6 s and 13 s. Figure 14 shows the lateral offset errors for the PI control and the proposed methods. The lateral offset errors of both methods increased due to the steering angle for the lane change at 6 s and 11 s, but they decreased by the differential braking inputs. Although the lateral offset error of the PI control decreased, but it was relatively larger than that of the proposed method because the steering angle cannot be rejected by the PI control method. On the other hand the lateral offset error of the proposed method was small because the steering angle was able to be rejected by the proposed method. Furthermore, the lateral offset error of the proposed method converged to zero rapidly. Figure 15 shows the vehicle trajectory of the proposed method. The dash-line represented the lane of the ego vehicle. The proposed method maintained the vehicle on the original lane under the steering angle for the lane change on the curved road.

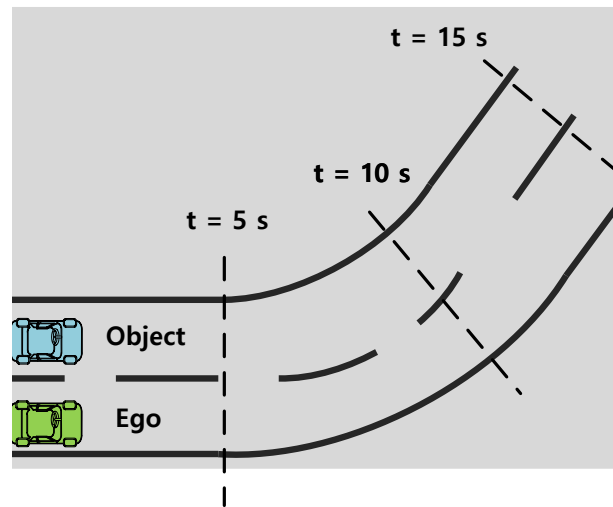


Figure 12. Curved Road.

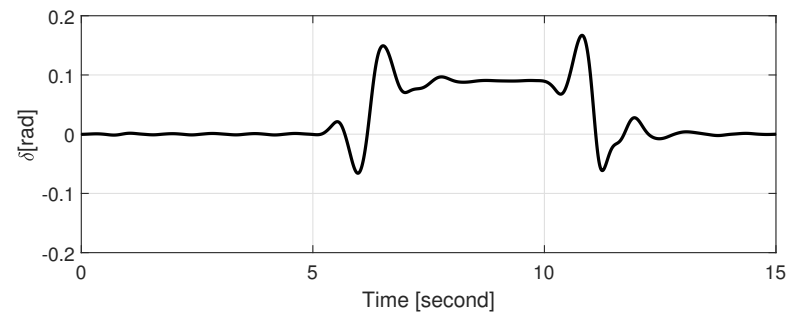
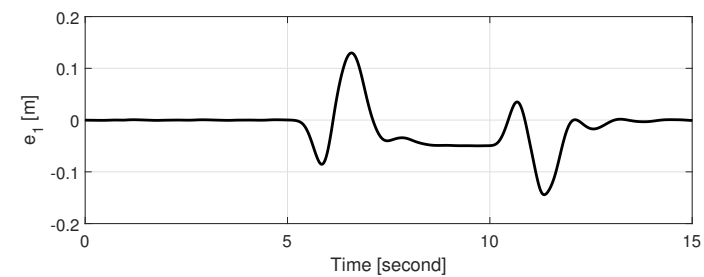
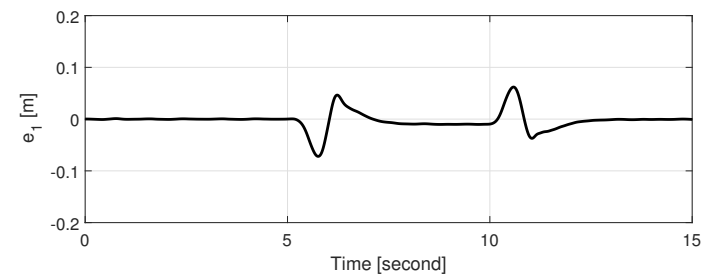


Figure 13. Steering angle.



(a) Lateral offset error of the PI control method e_1



(b) Lateral offset error of the proposed method e_1

Figure 14. Lateral offset errors for the PI control and the proposed methods.

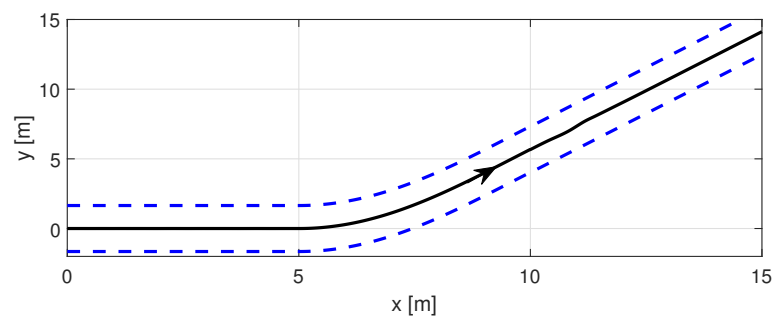


Figure 15. Vehicle trajectory of the proposed method.

6. Conclusions

A nonlinear differential braking control method to avoid collision of vehicles during lane change was proposed. The differential braking controller was designed based on sliding mode control and backstepping control schemes. Thus, the convergence of the lateral offset to zero under the steering angle can be guaranteed. The stability proof was mathematically proven using Lyapunov theory. The differential braking control system was designed to operate until the steering angle and lateral offset error were considerably small. The simulation results verified that regulation of the yaw rate and lateral position was improved by the proposed method for both straight and curved road. It was observed that the lateral control performance using differential braking under the driver torque was improved by the proposed method. In future work, we will aim to experimentally validate the performance of the proposed method using a test vehicle.

Author Contributions: Y.S.S. and W.K. designed the algorithm and developed the simulation; Y.S.S. and W.K. provided guidance in designing the algorithm; Y.S.S. and W.K. verified the simulation model and results. Both authors have read and agreed to the published version of the manuscript.

Funding: This research was supported by Basic Science Research Program through the National Research Foundation of Korea (NRF) funded by the Ministry of Education (2021R1A6A1A03043144).

Institutional Review Board Statement: Not applicable.

Informed Consent Statement: Not applicable.

Conflicts of Interest: The authors declare that they have no conflict of interest.

References

- Zhang, Y.; Jing, L.; Sun, C.; Fang, J.; Feng, Y. Human factors related to major road traffic accidents in China. *Traffic Inj. Prev.* **2019**, *20*, 796–800. [\[CrossRef\]](#)
- Shaon, M.R.R.; Qin, X.; Chen, Z.; Zhang, J. Exploration of contributing factors related to driver errors on highway segments. *Transp. Res. Rec.* **2018**, *2672*, 22–34. [\[CrossRef\]](#)
- National Highway Traffic Safety Administration. *Traffic Safety Facts 2005*; Department of Transportation: Washington, DC, USA, 2006.
- Jula, H.; Kosmatopoulos, E.B.; Ioannou, P.A. Collision avoidance analysis for lane changing and merging. *IEEE Trans. Veh. Technol.* **2000**, *46*, 2295–2308. [\[CrossRef\]](#)
- Laugier, C.; Paromtchik, I.E.; Perrollaz, M.; Yong, M.; Yoder, J.-D.; Tay, C.; Mekhnacha, K.; Nègre, A. Probabilistic analysis of dynamics scenes and collision risks assessment to improve driving safety. *IEEE Trans. Intell. Trans. Syst. Mag.* **2011**, *3*, 4–19. [\[CrossRef\]](#)
- Houénou, A.; Bonnifait, P.; Cherfaoui, V. Risk assessment for collision avoidance systems. In Proceedings of the 17th International IEEE Conference on Intelligent Transportation Systems (ITSC), Qingdao, China, 8–11 October 2014; pp. 386–391.
- Kim, J.; Kum, D. Collision risk assessment algorithm via lane-based probabilistic motion prediction of surrounding vehicles. *IEEE Trans. Intell. Transp. Syst.* **2017**, *19*, 2965–2976. [\[CrossRef\]](#)
- Gao, H.; Zhu, J.; Zhang, T.; Xie, G.; Kan, Z.; Hao, Z.; Liu, K. Situational assessment for intelligent vehicles based on Stochastic model and Gaussian distributions in typical traffic scenarios. *IEEE Trans. Syst. Man Cybern. Syst.* **2021**, 1–11. [\[CrossRef\]](#)
- Huang, M.; Gao, W.; Wang, Y.; Jiang, Z.P. Data-driven shared steering control of semi-autonomous vehicles. *IEEE Trans. Hum. Mach. Syst.* **2019**, *49*, 350–361. [\[CrossRef\]](#)
- Marcano, M.; Díaz, S.; Pérez, J.; Irigoyen, E. A review of shared control for automated vehicles: Theory and applications. *IEEE Trans. Hum. Mach. Syst.* **2020**, *50*, 475–491. [\[CrossRef\]](#)

11. Chen, Y.; Zhang, X.; Wang, J. Robust vehicle driver assistance control for handover scenarios considering driving performances. *IEEE Trans. Syst. Man Cybern. Syst.* **2021**, *51*, 4160–4170. [[CrossRef](#)]
12. Termous, H.; Shraim, H.; Talj, R.; Francis, C.; Charara, A. Coordinated control strategies for active steering, differential braking and active suspension for vehicle stability, handling and safety improvement. *Veh. Syst. Dyn.* **2019**, *57*, 1494–1529. [[CrossRef](#)]
13. Hajiloo, R.; Abroshan, M.; Khajepour, A.; Kasaiezadeh, A.; Chen, S.K. Integrated steering and differential braking for emergency collision avoidance in autonomous vehicles. *IEEE Trans. Intell. Transp. Syst.* **2021**, *22*, 3167–3178. [[CrossRef](#)]
14. Lin, Y.M.; Chen, B.C. Handling Enhancement of Autonomous Emergency Steering for Reduced Road Friction Using Steering and Differential Braking. *Appl. Sci.* **2021**, *11*, 4891. [[CrossRef](#)]
15. Lee, J.; Choi, J.; Yi, K.; Shin, M.; Kob, B. Lane-keeping assistance control algorithm using differential braking to prevent unintended lane departures. *Control Eng. Pr.* **2014**, *23*, 1–13. [[CrossRef](#)]
16. Pilutti, T.; Ulsoy, G.; Hrovat, D. Vehicle steering intervention through differential braking. *J. Dyn. Sys. Meas. Control* **1998**, *120*, 314–321. [[CrossRef](#)]
17. Uematsu, K.; Gerdes, J.C. A comparison of several sliding surfaces for stability control. In Proceeding of the International Symposium on Advanced Vehicle Control, Hiroshima, Japan, 9–13 September 2002; pp. 601–608.
18. Li, X.; Xu, N.; Guo, K.; Huang, Y. An adaptive SMC controller for EVs with four IWMs handling and stability enhancement based on a stability index. *Veh. Syst. Dyn.* **2021**, 1–24. [[CrossRef](#)]
19. Infinity, “Blind Spot Intervention” [Online]. Available online: [Http://www.infinitiusa.com/now/technology/blind-spot-intervention-system.html](http://www.infinitiusa.com/now/technology/blind-spot-intervention-system.html) (accessed on 15 May 2021).
20. Kim, W.; Chen, X.; Lee, Y.; Chung, C.C.; Tomizuka, M. Discrete-time nonlinear damping backstepping control with observers for rejection of low and high frequency disturbances. *Mech. Syst. Signal Process.* **2018**, *104*, 436–448. [[CrossRef](#)]
21. Park, J.-H.; Park, T.-S.; Kim, S.-H. Approximation-free output-feedback non-backstepping controller for uncertain SISO nonautonomous nonlinear pure-feedback systems. *Mathematics* **2019**, *7*, 456. [[CrossRef](#)]
22. Kang, C.M.; Kim, W.; Baek, H. Cascade backstepping control with augmented observer for lateral control of vehicle. *IEEE Access* **2021**, *9*, 45367–45376. [[CrossRef](#)]
23. Rajamani, R.; Tan, H.-S.; Law, B.K.; Zhang, W.-B. Demonstration of integrated longitudinal and lateral control for the operation of automated vehicles in platoons. *IEEE Trans. Control Syst. Technol.* **2000**, *8*, 695–708. [[CrossRef](#)]
24. Rajamani, R. *Vehicle Dynamics and Control*, 2nd ed.; Springer: Berlin/Heidelberg, Germany, 2012.
25. Ackermann, J. Robust car steering by yaw rate control. In Proceeding of the 29th IEEE Conference on Decision and Control, Honolulu, HI, USA, 5–7 December 1990; pp. 2033–2034.
26. Son, Y.S.; Kim, W.; Lee, S.-H.; Chung, C.C. Asynchronous sensor fusion using multi-rate kalman filter. *Trans Korean Inst. Elec. Eng.* **2014**, *63*, 1551–1558. [[CrossRef](#)]
27. Fayyad, J.; Jaradat, M.A.; Gruyer, D.; Najjaran, H. Deep learning sensor fusion for autonomous vehicle perception and localization: A review. *Sensors* **2020**, *20*, 4220. [[CrossRef](#)] [[PubMed](#)]
28. Lin, B.-F.; Chan, Y.-M.; Fu, L.-C.; Hsiao, P.-Y.; Chuang, L.-A.; Huang, S.-S.; Lo, M.-F. Integrating appearance and edge features for sedan vehicle detection in the blind-spot area. *IEEE Trans. Intell. Transp. Syst.* **2012**, *13*, 737–747.
29. Khalil, H. *Nonlinear Systems*, 3rd ed.; Prentice-Hall: Upper Saddle River, NJ, USA, 2002.
30. Cheng, H.-Y.; Jeng, B.-S.; Tseng, P.-T.; Fan, K.-C. Lane detection with moving vehicles in the traffic scenes. *IEEE Trans. Intell. Transp. Syst.* **2006**, *7*, 571–582.